SCALING OF THE EQUILIBRIUM SEDIMENTATION DISTRIBUTION IN DENSE DNA SOLUTIONS

S. TROHALAKI, A. A. BRIAN, H. L. FRISCH, AND L. S. LERMAN
Center for Biological Macromolecules, State University of New York at Albany, Albany, New York 12222

ABSTRACT DNA molecules, several persistence lengths long in sedimentation equilibrium at speeds high enough to maintain fairly close packing, show a dense, sharply-bounded turbid phase and an isotropic phase (as with shorter fragments) and also an intermediate, somewhat turbid region. The concentration distribution in the isotropic phase is in satisfactory agreement with a simple extension of scaled particle theory in which semiflexible chains are equivalent to straight rods of the same length. The net intermolecular interactions, as inferred from the Zimm cluster integral, are purely repulsive. As in our previous study with short fragments, the results are compatible with a hard-core electrostatic radius, decreasing with increasing salt concentration. However, for the longer fragments it is necessary to infer either a slightly greater mass per unit length or a slightly smaller electrostatic radius for closest agreement with scaled particle theory. The properties of the solution at the boundary with the turbid, presumably strongly ordered phase are consistent with those found for shorter fragments and with theoretical scaling expectation for a hard, asymmetric particle.

INTRODUCTION

We have examined the equilibrium distribution of moderately long DNA molecules in a centrifugal field at field strengths resulting in the close approach of helices, where the molecular separation is comparable with that of prokaryotic intracellular densities and intraviral packing. We find that the system resembles the packing behavior of short, rodlike helices, including a well-defined transition to an anisotropic phase (1), and the results permit a significant extension of scaled particle theory to somewhat flexible chains. However, the system behavior appears more complex than that consisting of shorter helices. Where single persistence length molecules separate into distinct isotropic and turbid phases, the longer molecules present, in addition, an intermediate, slightly turbid region.

EXPERIMENTAL

Molecules of the desired length distribution were prepared by shearing chicken erythocyte DNA in a rotating blade homogenizer (model 60K; Vir Tis Co., Inc., Gardiner, NY) at 20,000 rpm for 30 min in 1 M NaCl at 0° C. The solution was filtered, concentrated, and dialyzed to equilibrium against a flowing solution of each specified salt concentration. The length distribution after shearing was characterized by gel electrophoresis using the 22,125, 7,417, 5,801, 5,641, 4,876, and 3,524 base pair (bp) fragments of an EcoRI digest of lambda DNA, and the 1,410, 1,044, 919, 452, and 397 bp fragments of an Hae III digest of pBR322 as length standards for calibration of a conventional length-mobility function. The photographic density due to fluorescence of the ethidium-stained DNA was measured by a scanning microdensitometer and converted into DNA concentration using a somewhat arbitrary sensitometric function (2).

The fluorescence intensity along the lane containing the sample in the gel is shown in Fig. 1 *a*, and the distribution of the number of molecules of each length calculated from the scan is shown in Fig. 1 *b*. The number average length was 1,235 bp, roughly 8.4 persistence lengths, with half the modal peak height at 608 and 1,974 bp.

Samples were equilbrated in the centrifuge as described by Brian et al. (1). Each cell contained ~10 μl of solution, initially ~65 mg/ml. The extremely short optical path, ~0.1 mm, was measured by its interference pattern, as previously described. Scanning is carried out at wavelengths where the absorptivity of DNA is very low and also at wavelengths beyond the absorption band. The approach to equilibrium after each speed increment required ~1 wk in the centrifuge and was deemed adequate when scans at 24-h intervals agreed within 1% of the full-scale concentrations. It was not possible to achieve re-equilibration within reasonable times (3 wk) on descending from higher to lower speeds.

RESULTS

Representative scans at both 302 and 313 nm are shown in Fig. 2 for the sample equilbrated with 0.47 M NaCl. They indicate the presence of three distinguishable regions in the equilibrium distribution. There is no appreciable amount of DNA for the first 5.5 mm below the meniscus. The upper, low concentration region, I, ~1.5-cm wide, is free of light scattering as indicated by the low level of the 313-nm curve. It is convex upward in concentration vs. radius, opposite to the curvature of an ideal solution at sedimentation equilibrium. At ~3½ mm from the bottom of the cell, there is a sharp boundary in the scans at both wavelengths, below which the sample scatters light so severely that its concentration cannot be estimated, region III. Between the normal solution and the strongly scattering phase there is a distinct, bounded region, II, with higher apparent absorbance. However, the sudden increase in apparent absorbance at 302 nm between regions I and II is accompanied by a jump in the 313-nm profile. Because electronic excitation

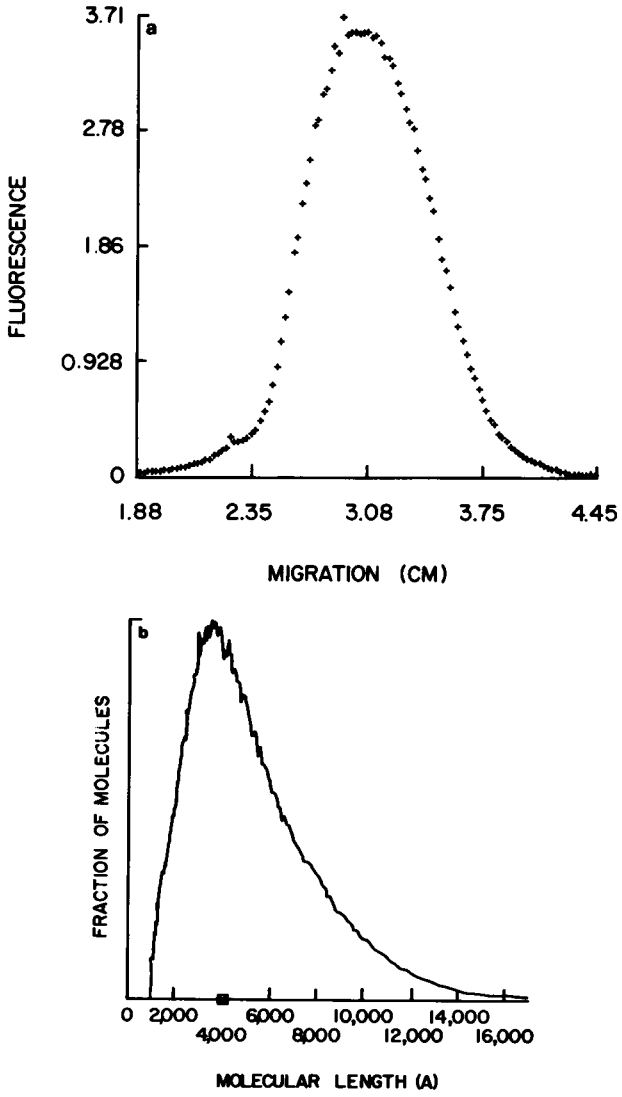

FIGURE 1 (*a*) Mass distribution of DNA after electrophoresis in agarose. The gel contained 5 μg sheared DNA and 5 mg/ml agarose. Electrophoresis was carried out at 1.4 v/cm for 10 h at 20°C. The gel was stained with ethidium and photographed in the conventional way. The lanes with the sheared DNA and the standard were scanned with a two-dimensional microdensitometer with a 100 μm (3) aperture. (*b*) Distribution of the number of molecules as a function of length. The number average length of 4,199 A is marked on the abscissa. Used as length standards were an EcoRI digest of lambda DNA (fragments 22,125, 7,417, 5,801, 4,876, and 3,524 bp), and an Hae I digest of pBR322 (fragments 1,410, 1,044, 919, 452, and 377 bp). The molecular length distribution was normalized to unity.

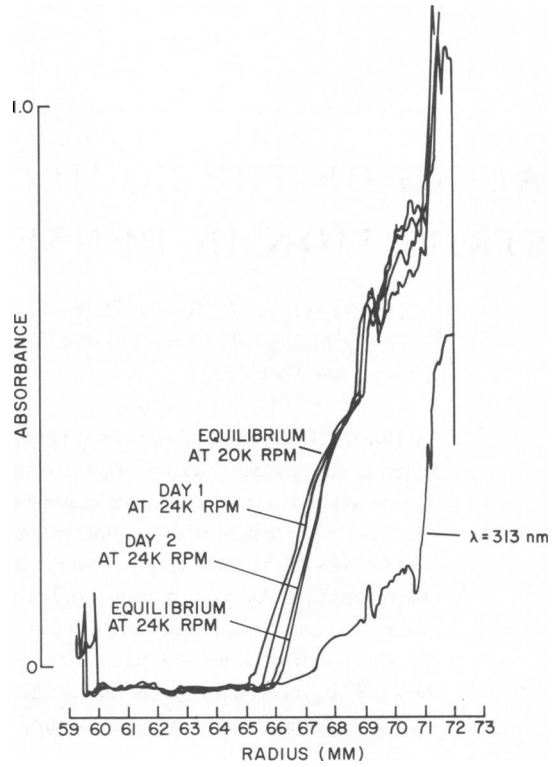

FIGURE 2 Distribution of DNA in the ultracentrifuge in 0.47 M NaCl as a function of distance from the rotor center. Scans showing the approach to sedimentation equilibrium at a rotor speed of 24,000 rpm were taken at 302 nm, where an absorbance of 1.0 represents a DNA concentration of 260 mg/ml. The bottom scan was taken at 313 nm where DNA absorbtivity is smaller by a factor on the order of 10.

makes a negligible contribution to the 313-nm measurement, we infer that the increment represents weak light scattering and characterizes a state of the solution different from that of either above or below the upper boundary. By scanning at several wavelengths above 302 nm and extrapolating according to the appropriate power law, the contribution of scattering to the apparent absorption could be estimated, permitting a reasonably reliable description of the DNA distribution in this region for the 2.0 M NaCl sample. Reduced osmotic pressure as a function of concentration was calculated from the distribution in region I, as previously described (1), and for regions I and II for the 2.0 M NaCl sample.

DISCUSSION

The Zimm clustering function (3), shown in Fig. 3 for the solution equilbrated with 2.0 M NaCl, decreases monotonically, indicating that the net interhelical forces are exclusively repulsive, despite strong electrostatic screening by concentrated salt. Exclusively repulsive interactions are found also for the other salt concentrations.

Our previous study (1) showed a close correspondence between the experimental osmotic pressure of 145 and 200 bp fragments as a function of concentration and the theoretical function based on a one-component gas of rigid spherocylinders, providing that an appropriate value was taken for the radius of the cylinder. Because the rms end-to-end length is expected to be ~0.82 of the contour length for 200 bp molecules, the correspondence with theoretical behavior based on straight rods is plausible. However, where the contour length is an order of magnitude larger than the persistence length, the suitability of simple scaled particle theory is not obvious. For molecules with the number average length of our preparation, ~8.4 persistence lengths, the average angle between the helix

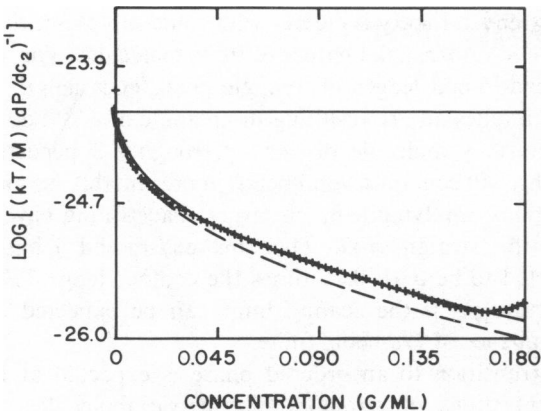

FIGURE 3 Log of the clustering function vs. DNA concentration for the 2.0 M NaCl sample at 20,000 rpm. points (+) calculated from the experimental data and the solid curve (–) drawn according to SPT using a molecular weight of 3.80×10^{-3} and a hard-core radius of 10.6 A. The dashed line (– – –) is drawn using the same molecular weight but with the radius found for single persistence length DNA. The solid horizontal line represents ideal solution behavior. Every third experimental point is plotted.

axes of the first and last segments is close to the limiting value for random chains, 90°, and the rms end-to-end distance is 0.46 of the contour length.

To extend the theoretical treatment to this system of semi-flexible macromolecules, we employ a scaling concept due to Grosberg and Khokhlov (4) among others. (See also the work of Flory [5] and de Gennes [6].) They argue that the same definition of the asymmetry parameter, the ratio of the contour length, L, to the hard-core radius, a, remains applicable in longer molecules despite the flexibility, provided that the ratio of the persistence length, ℓ, to the hard-core radius is sufficiently large; the functional relation between asymmetry, concentration, and osmotic pressure then remains unchanged for an isotropic fluid. This can be seen intuitively in that interactions between the helices occur on a scale of the order of the hard-core radius, while effects of flexibility arise only on the scale of the persistence length, ℓ. Thus, our previous scaled particle equation for single persistence length fragments should apply if ℓ/a is replaced by L/a.

TABLE I

LENGTHS AND ASYMMETRICS INFERRED FROM THE CORRESPONDENCE OF THE DISTRIBUTION OF DNA IN THE NONTURBID, UPPERMOST PHASE WITH SCALED PARTICLE THEORY

NaCl*	a_o‡	L_1/a_o§	L_1‖	N_1¶	t_1**
M	*Å*		*Å* $\times 10^{-3}$	*bp*	*Å*
0.47	16.0	90	1.45	473	3.06
0.73	14.3	117	1.63	545	2.99
1.0	13.0	80	1.04	363	2.86
2.0	11.7	105	1.22	400	3.06

Assuming that the hard-core radii are fixed at the values previously found (Brian et al. [1]) for single persistence length particles. The asymmetry and molecular weight (as base pairs) tabulated provide the closest fit to the theoretical function.

*Concentration of the equilibrium dialysate.

‡Hard-core radius found previously (1) for single persistence length fragments.

§SPT asymmetry found, assuming the hard-core radius is fixed at a_o.

‖Average effective particle length, as given in the second and third columns.

¶Number of base pairs per particle corresponding to the mass concentration and adjusted particle density.

**Effective length per base pair.

Close correspondence between experimental osmotic pressure as a function of concentration and the extended scaled particle equation was achieved by two methods. First, assuming that the same effective electrostatic radii found for single persistence length particles (1) are valid for the longer molecules, the data were fit with the radii fixed at the short rod values. The length and molecular weight were then adjusted independently to a minimal χ^2. This effectively relaxed the conventional proportionality between length and molecular weight for B DNA: 3.4 Å/bp. Molecular weight enters the SPT formulation

$$\frac{P}{\rho k_B T} = \frac{1 + B + C + D + (B + C)^2 + \frac{1}{3} D\,(B + \frac{3}{2} C)}{(1 - B - C)^3},$$

where $B = \pi a^3 \rho\,(L/a)$, $C = \frac{4}{3}\pi a^3$, and $D = \frac{1}{2}\pi a^3 \rho\,(L/a)^2$ in relating particle concentration, ρ, to mass concentration as measured. The fit demands a larger mass per unit length varying from 2.86 to 3.06 Å/bp. Values of effective particle length and molecular weight corresponding to a best fit of the data are presented in Table I, along with the asymmetries and effective lengths per base pair.

The second method used to fit the data to the theoretical function involves independent adjustment of contour length and hard-core radius while retaining a fixed unit length of 3.4 Å/bp. The fit for the 2.0 M NaCl sample is

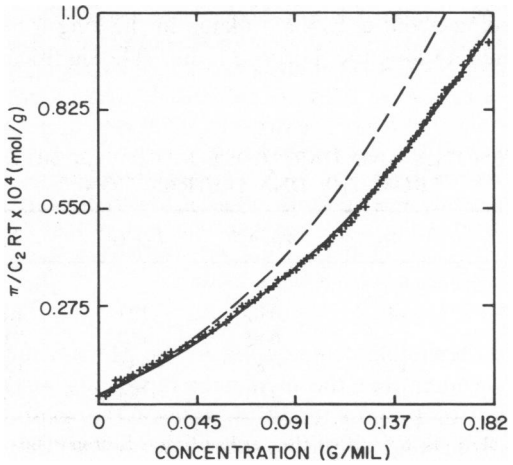

FIGURE 4 Reduced osmotic pressure as a function of DNA concentration for the 2.0 M NaCl sample at 20,000 rpm. Every third point (+) is plotted. The solid curve (–) is drawn according to SPT using a molecular weight of 3.80×10^{-3} and a hard-core radius of 10.6 A. The dashed line (– – –) is drawn using the same molecular weight but with the hard-core radius found for single persistence length DNA.

shown in Fig. 4. The goodness of fit is slightly better than that described above, a standard error 18% smaller. Values of the contour length and hard-core radius derived in this way are given in Table II, together with the corresponding radii for single persistence length fragments presented by Brian et al. (1) or interpolated from that data. Our radii are systematically smaller, but not implausibly low. The fitted lengths are not uniform and are less than one-half the number average length value calculated from the gel distribution. The molecular weights are larger than those in Table I, corresponding to a lower particle density.

The theoretical partitioning of rodlike molecules according to size between isotropic and anisotropic phases of a dense, polydisperse solution, corresponding in principle to the present system, has been studied by Flory and Frost (8). For an athermal system consisting of the most probable distribution of particle lengths, all with an axial ratio of eight and equal volumes in the two phases, the expected number average molecular weight will be three times as high in the anisotropic phase as in the isotropic phase. Since our distribution, as seen in Fig. 1 *b*, is not far from the most probable (our polydispersity is 1.7; that of the most probable distribution is 1.88), a partitioning to this extent may account for the difference between the overall number average molecular length we estimate by gel electrophoresis of the original polydisperse preparation and the values that are inferred from the sedimentation equilibrium in the isotropic phase. For a Poisson distribution of lengths, which is sharper than the most probable, Frost and Flory (9) find a smaller ratio, 1.35, between the number average lengths in the two phases.

Accepting the smaller mean particle length, the distribution in the fully isotropic phase is accommodated to SPT expectation, (as extended by Grosberg and Khokhlov [4]) either by accepting a smaller effective radius than was found appropriate for single persistence length rods or by introducing about a 12% shrinkage in the length-to-mass ratio and retaining the short rod radius. The significance of the extended theory is clearer with some representation of the three-dimensional nature of these molecules. The average end-to-end length of a single persistence length segment implies an arc resulting in an angle of ~70 between the ends. A molecule of 445 bp, roughly 3 persistence lengths, will contain several bends in presumably unrelated directions, implying a much larger space-filling envelope than the straight rod. The rms end-to-end length is expected to be 0.61–0.75 times the contour length. Some departure from the scaling limit can be expected as a consequence of ℓ/a being finite.

TABLE II
LENGTHS AND HARD-CORE RADII INFERRED FROM THE DNA DISTRIBUTION

NaCl*	A_2‡	A_2/a_0§	L_2/A_2‖	L_2¶
M	Å			Å × 10^{-3}
0.47	14.2	0.89	127	1.80
0.73	12.1	0.85	170	2.06
1.0	10.5	0.81	135	1.41
2.0	10.6	0.91	184	1.95

As in Table I, assuming that the particle length is proportional to the molecular weight, with 3.4 Å per base pair.
*Concentration of the equilibrium dialysate.
‡Hard-core radius according to the extended scaled particle theory.
§Ratio of hard-core radius (as in the second column) to value found by Brian et al. (1).
‖Asymmetry according to extended scaled particle theory.
¶Particle length according to extended scaled particle theory.

A transition to an ordered phase is expected at high concentrations of strongly asymmetric molecules. The parameters for this transition for single persistence length DNA helices are within the limits expected theoretically, and we have argued that the turbidity of the dense phase is explicable as highly ordered cholesteric packing (1).

Because the turbidity of region II makes a small contribution to the total apparent absorbance, an acceptable estimate of the DNA distribution can be made using an approximate turbidity correction by extrapolation from the wavelengths at which DNA has negligible absorption. Measurements at 313, 334, 365, or 404 nm, taken under conditions only slightly different from the present set of equilibria, follow an inverse 3.2 power dependence on wavelength, independent of salt. Extrapolation to 302 nm for 2.0 M salt gives the same scattering increment as that indicated at the sharp boundary between region II and the isotropic solution in region I. The extrapolated corrections were applied to the lower salt samples, in which the boundary was somewhat more diffuse. Because the corrected DNA distribution for the 2-M sample follows the SPT function calculated from region I with no significant change of parameters, it seems appropriate to regard regions I and II as a single phase, and we presume that SPT provides an appropriate description of the properties determining the transition to the highly turbid, sharply bounded phase in region III for all samples.

Although we are unable at present to account for the nature of region II, it has at least some properties resembling a stable phase. The upper boundary is seen as a distinct inflection in the scan of apparent absorbance at all salt concentrations and both wavelengths. Grosberg and Khokhlov (4) have suggested that one or more partially ordered phases may fulfill stability criteria within a formulation based on a potential of mean force.

We can compare the present results with the previous work on small molecules, assuming that the phase boundary at the top of region III is similar, despite whatever difference determines weak turbidity in region II. The volume fraction of solute just above the phase boundary, the critical value, can be calculated from the corrected concentration and the volume of cylinders of the appropriate contour length using the hard-core radius inferred from the scaled particle fit. The critical volume fraction for long chains is 0.18–0.21, independent of salt concentration,

calculated with a contour length of 3.4 Å/bp, or 0.22 to 0.25 with the standard radii and shorter, adjusted contour lengths. The values are included in Table III. Persistence length rods gave values of 0.26 and 0.24 in 1.0 and 2.0 M NaCl, respectively. Slightly smaller values are expected for the longer helices (7, 10, 11); the independence of the critical volume on the salt concentration is expected from scaling theory.

Although the opacity of the ordered phase precludes direct measurement of the DNA concentration, an average value in region III is estimated from the starting total amount, the shape of the centrifuge cell, the position of the boundary, and the integrated distribution in the measurable regions. The ratio of the average in the ordered phase to the critical concentration above the boundary can be compared with the ratio of concentrations in equilibrium at the boundary. Our values will necessarily be larger than the ratio at the boundary because the denser solution below the boundary is included in the averaging. We find a value of 1.48 for the sample in equilibrium with 2.0 M NaCl. The boundary ratio obtained by Flory and Ronca (12) by a lattice model approximation, is 1.47. Onsager (7), who used the second virial approximation and the variational method, obtained a value of 1.34. Eliminating the approximation due to the variational method, Kayser and Raveche (13) obtained a ratio of 1.28. Because our experimental ratio overestimates the ratio of boundary concentrations it is less compatible with the lattice model than with the latter two.

The scattering profile of region III as shown in Fig. 2 consists of two parts: moderate scattering from the phase boundary at ~69 down to 71 mm, then considerably stronger scattering from 71 mm to the outer edge of the cell. The jump is discernible at all salt concentrations. The effect suggests that there may be a second transition within the anisotropic phase. We have had hints of a transition in other studies, for example, in an abrupt change in the width of the diffraction peak corresponding to interhelical scattering (14).

TABLE III

VOLUME FRACTION OF PARTICLES IN THE LESS TURBID PHASE ADJACENT TO THE BOUNDARY WITH THE ANISOTROPIC, STRONGLY SCATTERING BOTTOM PHASE*

NaCl	0.47 M	0.73 M	1.0 M	2.0 M
Φ_1‡	0.24	0.23	0.25	0.22
Φ_2§	0.21	0.18	0.19	0.20
Φ^*‖	—	—	0.26	0.24

*The volume fraction was calculated from the relation $\Phi = C\pi N_{av}A^2(L_2 + 4/3A)/MW$, when C is the mass concentration and N_{av} is the number of particles per mole.

‡Φ_1 uses the lengths and radii, L_1 and a_0, presented in Table I.

§Φ_2 uses the lengths and radii, L_2 and A_2, presented in Table II.

‖Φ^* is the volume fraction at the boundary found by Brian et al. (1) for single persistence length particles.

CONCLUSIONS

This study, which extends the theoretical treatment of rigid rods of Brian et al. (1) to a system of semi-flexible macromolecules, is in reasonably good agreement with the application of scaling concepts to a long, wormlike chain, which in the limit of ℓ/a, is expected to behave in isotropic solution like a straight rod with the same contour length. The slightly smaller effective length per base pair (Table I) or the somewhat smaller hard-core radii presented here (Table II) as compared with those found for single persistence length fragments may be a consequence of the finite ℓ/a, far from the scaling limit. We believe that the transition to an anisotropic phase observed here is the same as that observed with single persistence length fragments (1). The parameters for this transition are consistent with those found for the short rods, together with theoretical treatments of asymmetric hard-core fluids (7, 10, 11). There is evidence that longer molecules in the original polydisperse preparation are preferentially segregated into the anisotropic phase. The presence of light scattering in region II, may imply a partial ordering, as suggested by Grosberg and Khokhlov (4).

We would like to express our appreciation to Karen Silverstein and Ian Hurley for their help in computing and laboratory matters, to John Dugan for assistance with instrumentation, and to Nelly Brown for assistance in preparing this manuscript.

This work was supported by grants DMR 780593804 and PCM 7920672 from the National Science Foundation.

Received for publication 21 June 1983 and in final form 30 September 1983.

REFERENCES

1. Brian, A. A., H. L. Frisch, and L. S. Lerman. 1980. Thermodynamics and equilibrium sedimentation analysis of the close approach of DNA molecules and a molecular ordering transition. *Biopolymers.* 20:1305–1328.
2. Fischer, S. G., and L. S. Lerman. 1980. Separation of random fragments of DNA according to properties of their sequences. *Proc. Natl. Acad. Sci. USA.* 77:4420–4424.
3. Zimm, B. H. 1952. Simplified relation between thermodynamics and molecular distribution functions for a mixture. *J. Chem. Phys.* 21:934–935.
4. Grosberg, A. Yu., and A. R. Khokhlov. Some Problems of the Statistical Theory of Polymeric Lyotropic Liquid Crystals, International Atomic Energy Agency and UNESCO International Center for Theoretical Physics, *Internal Report, IC/80/71,* June 1980. Miramore-Trieste.
5. Flory, P. J. 1953. Principles of Polymer Chemistry. Cornell University Press, Ithaca, NY.
6. de Gennes, P. G. 1979. Scaling Concepts in Polymer Physics. First ed. Cornell University Press, Ithaca and London. 324.
7. Onsager, L. 1949. The effects of shape on the interaction of colloidial particles. *Ann. NY. Acad. Sci.* 51:627–659.
8. Flory, P. J., and R. S. Frost. 1978. Statistical thermodynamics of mixtures of rodlike particles. 3. The most probable distribution. *Macromolecules.* 11:1126–1133.
9. Frost, R. S., and P. J. Flory. 1978. Statistical thermodynamics of

mixtures of rodlike particles. 4. The Poisson distribution. *Macromolecules.* 11:1134–1138.

10. Flory, P. J. 1956. Phase equilibria in solutions of rodlike particles. *Proc. R. Soc. Lond. Ser. A.* 234:73–89.
11. Lasher, G. 1970. Nematic ordering of hard rods derived from a scaled particle treatment. *T. Chem. Phys.* 53:4141–4146.
12. Flory, P. J., and G. Ronca. 1979. Theory of systems of rodlike particles. 1. Athermal systems. *Mol. Cryst. Liq. Cryst.* 54:289–309.
13. Kayser, R. F., Jr., and H. J. Raveche. 1978. Bifurcation in Onsager's model of the isotropic–nematic transition. *Phys. Rev. A.* 17:2067–2072.
14. Maniatis, T. P., J. H. Venable, Jr., and L. S. Lerman. 1974. The structure of ψ DNA. *J. Mol. Biol.* 84:37–64.